HHS Public Access

Author manuscript

Nat Neurosci. Author manuscript; available in PMC 2009 August 31.

Published in final edited form as:

Nat Neurosci. 2008 December ; 11(12): 1419–1429. doi:10.1038/nn.2225.

Continuous shifts in the active set of spinal interneurons during changes in locomotor speed

David L. McLean[1], **Mark A. Masino**[1,#], **Ingrid Y. Y. Koh**[2], **W. Brent Lindquist**[2], and **Joseph R. Fetcho**[1,*]

[1]Department of Neurobiology and Behavior, Cornell University, Ithaca, NY

[2]Department of Applied Mathematics and Statistics, Stony Brook University, Stony Brook, NY

Abstract

The classic 'size principle' of motor control describes how increasingly forceful movements arise by the recruitment of motoneurons of progressively larger size and force output into the active pool. Here, we explore the activity of pools of spinal interneurons in larval zebrafish and find that increases in swimming speed are not associated with the simple addition of cells to the active pool. Instead, the recruitment of interneurons at faster speeds is accompanied by the silencing of those driving movements at slower speeds. This silencing occurs both between and within classes of rhythmically-active premotor excitatory interneurons. Thus, unlike motoneurons, there is a continuous shift in the set of cells driving the behavior, even though changes in the speed of the movements and the frequency of the motor pattern appear smoothly graded. We conclude that fundamentally different principles may underlie the recruitment of motoneuron and interneuron pools.

Vertebrates can produce movements of widely varying strengths and speeds. Much of our understanding of how this is accomplished comes from decades of work on the recruitment patterns of motoneurons in the spinal cord1-3. These studies have revealed a universal principle of motor control, the size principle, which relates the order of recruitment of motoneurons to features such as axon conduction velocity and motor unit force, which are correlated with measures of cell size in motoneurons 4, 5. According to the size principle, the pool of active cells steadily increases in size with progressive increases in the force and speed of movement, with faster motoneurons and motor units added to the set of motoneurons active in weaker or slower movements. This pattern appears to be widespread among both vertebrates and invertebrates 6-8, confirming the size principle as a general feature of motor organization.

Much less is known about how interneurons are recruited during increases in the strength, speed, or frequency of movements. Although there are classic studies of the spinal central pattern generators (CPGs) that drive rhythmic movements 9-12, historically these studies

*Correspondence to JRF: e-mail, jrf49@cornell.edu, Tel, 607 254-4341, Fax, 607 254-1303..

#Current address: Department of Neuroscience, University of Minnesota, Minneapolis, MN.

focused on locomotion during periods of steady of motor output 13-17. Consequently, with a few exceptions 18-20, prior work has focused mostly on the structure of the pattern generating networks, rather than on recruitment patterns.

We have been studying the spinal circuits responsible for swimming in larval zebrafish to ask how the recruitment of identified premotor interneurons varies with speed and how this compares to the classic recruitment pattern of motoneurons. We showed previously that there is a topographic map of recruitment of motoneurons and premotor excitatory interneurons in which the most ventral motoneurons and interneurons are recruited at the lowest swimming frequencies, with increasingly dorsal ones becoming active at higher and higher frequencies based upon their location. While both the motoneurons and interneurons followed the same dorsoventral topography of initial recruitment, there were indications that, once recruited, the two populations showed very different activity patterns as the frequency of swimming increased.

Here, we show that there is indeed a substantial difference in the way excitatory interneuron and motoneuron pools are recruited. Among the motoneurons, as the frequency of swimming increases, those recruited at lower frequencies remain active at higher ones, leading to an increasingly expanding pool of active cells. This is the typical size principle pattern. The recruitment of interneurons, on the other hand, is not associated with the simple addition of more interneurons to those already active at lower speeds; instead, the recruitment of new interneurons is accompanied by the silencing of premotor interneurons driving movements at lower speeds.

This pattern, in which a new regime of neurons is recruited as the older ones are silenced, is observed both between and within classes of interneurons. A premotor excitatory class that is active at slow speeds (MCoDs) is turned off at higher speeds when a new excitatory premotor class is engaged (CiDs). Even within one class (CiDs), the recruitment of new members with increasing frequency of bending occurs as those cells previously recruited are gradually removed by inhibition. These continuous shifts in the cells driving the behavior occur even though changes in the frequency of the motor pattern and the frequency of bending movements appear smoothly graded. We conclude that the recruitment of interneuron pools differs in an important respect from that of motoneurons, suggesting that different organizational principles underlie the function of the two populations.

Results

Gradation of movements

Larval zebrafish spend most of their time swimming around slowly and spontaneously in brief bouts, with bending occurring primarily at the tail 21. These bends are accompanied by alternating movements of the pectoral fins 22. The larvae can, however, move very quickly when touched and these movements involve bending along much of the body, with the pectoral fins held against the abdomen 21, 22. We initially asked whether these different movements of the body were discrete patterns or instead represented the ends of a continuum of movements. We did this by exploring the kinematic patterns in cases in which

the animal made transitions from moving quickly to moving slowly, because we could more reliably elicit bouts of swimming characterized by decelerations in speed.

Fish were stimulated by a touch on the tail, filmed at 1,000 frames a second, and the bending at different places along the body was then quantified automatically by software that tracked the midline of the fish. The fish appeared to grade smoothly from fast bending movements initially in response to the touch to slow ones at the end of a swimming bout, as shown by the images in Figure 1a. During the initial movements, there was bending all along the body, as shown by the plots of body yaw in Figure 1b. As the fish slowed, the bending at the head was reduced to zero, while tail bending still remained. An analysis of the amount of yaw at the head and the tail at different frequencies of swimming from 12 trials of evoked swimming, one from each of 12 fish (Fig. 1c), showed that the frequency of bending in the evoked responses ranged from over 70 Hz down to about 20 Hz. At the lowest frequencies, the head typically showed no yaw, while tail yaw persisted. We also examined the pattern of bending during spontaneous, slow swimming (12 episodes in the same 12 fish), as in Figure 1d, for comparison to the evoked swimming. The bending during slow swimming looked identical to the pattern of bending at the end of the evoked swimming episodes, with no head bending and substantial tail movements. These observations are based on decelerations in swimming speed, which were easier to elicit. However, we did observe rare accelerations in swimming speed. The movements in these transitions from slow to fast were also smoothly graded, with head movements increasing with speed (not shown). Collectively, these data indicate that the fish can smoothly grade between the fastest and the slowest swimming movements without any obvious discontinuity in the axial bending pattern.

Gradation of the motor pattern

We next asked whether the smooth gradation of movement frequency and bending in movements evoked by a brief electrical stimulus was reflected in a smooth gradation of the motor pattern. We recorded fictive motor patterns from motor nerves at two different places along the body in paralyzed fish in 10 trials, one from each of 10 fish, as in Figure 1e. Quantification of the burst pattern, shown in Figure 1f, revealed that the burst frequency could grade smoothly from high frequency at the beginning of a bout to low at the end. The intersegmental delay (Fig. 1g) varied with cycle period, with increased delays as the movement frequency slowed, as is typical of swimming. The slope of the relationship, however, appeared to change over the range of swimming, with the slowest swimming having especially long delays that correlated less with frequency than those at faster swimming speeds. Even though there is little rostral bending at slow swimming speeds, there was still evidence of rostral motor activity over the range of movement frequencies, with comparable burst frequencies at both the head and the tail (Fig. 1e, bottom).

These data indicate that the motor pattern, like the movements, can be smoothly graded from fast to slow frequencies. Even though there is no yaw of the head at the slowest swimming speeds, there is nonetheless both rostral and caudal motor output, as at higher frequencies of bending. This suggests that at slow speeds there is not enough activity rostrally to move the relatively more massive front of the fish, even though the tail is moving substantially.

Recruitment of motoneurons

In an earlier study, we showed that the lowest swimming frequency at which a motoneuron becomes active is topographically related to its position in the spinal cord 23. Ventral motoneurons are first recruited at low frequencies with increasingly dorsal ones recruited as the frequency of swimming increases. If these cells follow the classic size principle, we would expect that as new motoneurons are added at higher frequencies, those already recruited would remain active, so the active pool would increase in size as the frequency of swimming increased. We examined this by looking at motoneurons from the data set in our previous study 23 and asked here if the more ventral neurons, initially recruited at low frequencies, remain active at higher ones.

Figure 2 shows images of motoneurons located at different dorso-ventral locations in spinal cord (Fig. 2a, f, k), along with patch recordings of their rhythmic firing activities during fictive swimming, measured from motor nerves (Fig. 2b, g, l). Primary motoneurons are a distinctive class and are distributed in most dorsal cord (Fig. 2c). Secondary motoneurons are more broadly distributed in the dorso-ventral plane, so we arbitrarily divided them into dorsal and ventral groups based on an average value of their position (0.42 ± 0.02, $n = 30$; Fig. 2h, m). The physiology and counts of spike number versus swimming frequency (Fig. 2i, n) showed clearly that the secondary motoneurons continue to fire even at the fastest frequencies of swimming, There is a decline in the number of spikes per burst in the smallest motoneurons with increasing frequency that is probably the result of a decrease in the duration of the swimming bursts at higher frequencies, which allows for fewer spikes per burst. Even though the number of spikes per cycle is lower at high frequencies of swimming, the fidelity of the firing of the smallest motoneurons (measured as the percentage of cycles in which they are active) rises to 100 % at the highest frequencies (Fig. 2j, o). They do not shut off, but fire more consistently as frequency rises. Primary motoneurons are initially recruited at somewhat higher frequencies, but they too continue to fire at even higher swimming frequencies (Fig. 2d, e). We conclude based upon this, along with a size relationship established in our prior work 23, that the motoneurons behave in accord with the classic size principle. They are recruited largely by size and the active pool grows with increases in frequency of swimming as more and more neurons are added and remain active. In the following sections, we explore the recruitment of the excitatory interneurons that drive motoneurons. These are recruited from ventral to dorsal like motoneurons as we described previously 23 but their recruitment differs from motoneurons in other, very important respects.

Morphology of interneurons (MCoDs) active at slow speeds and their outputs to motoneurons

Two classes of rhythmically active excitatory interneurons have been identified in zebrafish: circumferential descending interneurons (CiDs) and multipolar commissural interneurons (MCoDs). Prior work revealed the distribution of the CiD interneurons and their direct connections with motoneurons 24, 25. Less was known about the distribution of the outputs from the MCoDs and whether they also connect directly to motoneurons. Because their premotor status was important for this study, we examined their morphology and connectivity as a basis for studying how this pool is recruited relative to the CiDs. Earlier

work using either *in vivo* imaging 26 or patch recordings and ablations 23 showed that the MCoDs, were active during low frequencies of swimming and were important for its generation. As described previously 27, MCoD neurons have ventral somata located laterally in the neuropil and a commissural axon that descends in the ventral spinal cord (Fig. 3a, b). Our electroporations of single cells revealed that MCoDs have short, finger-like axon collaterals that arise from the main axon, as in Figure 3a and c.

To examine the branching patterns of MCoDs at different rostrocaudal positions, we electroporated individual neurons with dye and reconstructed the entire axonal arbor of 22 neurons in three dimensions (Fig. 3d, e). The total branch length in three dimensions (including the main axon) in each segment was quantified and the length within a segment was plotted as a function of segment number for cells at different rostrocaudal positions, as in Figure 3e. These data revealed that rostral neurons had more extensive branching in rostral regions of the spinal cord, with gradually reduced branching toward the tail (Fig. 3e, top). The opposite was true for caudal neurons, which branched more strongly in the tail than in the initial portion of their axons (Fig. 3e, bottom). The result was that the population as a whole had outputs distributed all along the spinal cord.

Electroporation of pairs of neurons in different colors, showed that although the regions of their branches sometimes overlapped, they often branched in different locations (Fig. 3f, g). We noticed in more rostral regions of the spinal cord that these branches were often in close proximity to cell bodies located laterally in the neuropil, identified using DIC optics (Fig. 3h-j). This is where MCoDs are typically found, and we confirmed the proximity of MCoD collaterals to other MCoDs by pairwise filling of electroporated MCoDs with back-filled MCoDs in a different color (Fig. 3k-n). The likelihood that rostral MCoDs were providing drive to other MCoDs (as indicated by their more rostral branching) could explain why ablation of relatively small numbers of rostral MCoDs in prior studies could have clear effects on slow swimming 23. Pairwise filling of MCoDs with GFP-labeled motoneurons also revealed close apposition of MCoD axonal branches to small, ventral secondary motoneurons all along the spinal cord (Fig. 3o-q, r-t). Together the morphology indicates that the MCoDs are positioned to drive motor output from smaller ventral motoneurons throughout the spinal cord, and to excite one another. This is consistent with the broad rostrocaudal activity recorded during slow swimming, even though the movement itself is largely in the tail region at slow speeds.

Previous *in situ* staining indicated that MCoDs expressed a vesicular glutamate transporter and were probably glutamatergic 28. To confirm the transmitter phenotype and establish connectivity with motoneurons, we recorded from MCoD/motoneuron pairs (n = 4), as in Figure 4a. Firing an action potential in the MCoD led to a postsynaptic potential in small ventral motoneurons with an initial small, shorter latency depolarization, followed by a slightly longer latency and larger depolarization, as shown at the top of Figure 4b. We tested the monosynaptic nature of the connection by raising magnesium and calcium concentrations to lower excitability and block polysynaptic pathways, as in the middle panel of Figure 4b. In these cases (n = 3), the responses persisted, consistent with a monosynaptic connection 29. The longer latency postsynaptic responses were blocked by a mixture of NBQX and APV (n = 3), leaving only the small, shortest latency component (bottom trace

of Fig. 4b). This short latency component followed spikes generated in the MCoDs at very high frequencies (up to 245 Hz) with no jitter. The later component failed at these high frequencies (not shown). The initial response was therefore likely to be an electrotonic connection, which was followed by a glutamatergic response. The delay from the electrotonic start to the beginning of the chemical response was 0.67 ± 0.07 ms (n = 4), consistent with the latency of a monosynaptic chemical synapse. Although the combined use of NBQX and APV prevents us from determining whether the glutamatergic response is via AMPA or NMDA receptors, the collective evidence is consistent with a mixed electrotonic and chemical synapse from the MCoDs onto ventral motoneurons. The axons three of the four motoneurons were intact and could be traced to axial muscle. The MCoDs thus monosynaptically excite small ventral axial motoneurons.

Inhibition of the class of MCoD premotor interneurons as the frequency of swimming increases

The MCoD interneurons are recruited at the lowest frequencies of swimming, with considerable activity during the spontaneous bouts of swimming typical of most larval swimming behavior (Fig. 5a, b). While MCoDs fire consistently at the lowest swimming frequencies during motor activity in fictive preparations, the number of spikes drops as swimming frequency rises until the neurons are no longer active at higher frequencies. This is shown for a single neuron in Figure 5c, and quantitatively for data from 10 larvae in Figure 5d and e. The number of spikes in all cells was zero at frequencies of about 50 Hz and above, although individual neurons could drop out well before that, as in Figure 5c. The MCoD activity declines substantially over the frequency range in the vicinity of 40 Hz and above, where the fish typically switch from slow swimming involving axial and pectoral fin movements to fast swimming involving just axial muscle (low end of the behavioral switch is 36 Hz per 22).

During swimming evoked by electrical stimulation, the MCoDs were typically silent at the beginning of the bout, when the swimming frequency was highest, and became active later as the frequency slowed, as in Figure 6a and b. This pattern occurred both in cell-attached (Fig. 6c) and whole-cell recordings (Fig. 6d), indicating that it did not result from an alteration of membrane potential or cellular properties produced by perfusion of the neuron with our intracellular patch solution. The absence of activity during the high swimming frequencies early in an evoked swimming bout was accompanied by a hyperpolarization of the MCoD that was made more evident by depolarizing the cell (Fig. 6a, b, arrow). We applied 1 μM strychnine (n = 6) to test for a role of glycinergic inhibition in the production of the hyperpolarization. This led initially to a recovery of rhythmic activity early in evoked bouts (Fig. 6e, control; 6f strychnine) followed, in bouts elicited after extended perfusion, by sustained activity without the bursting pattern of swimming (Fig. 6g). The early inhibition of activity returned when the drug was removed (Fig. 6h). The fact that MCoDs can fire rhythmically at fast speeds in the presence of strychnine suggests that MCoDs are receiving phasic excitatory drive, but that it is masked by glycinergic inhibition. These observations are consistent with the idea that the absence of activity early in the bout was a consequence of glycinergic inhibition of the neurons at higher swimming frequencies, which was reduced at lower frequencies of swimming when the neurons are active.

The activity of members of another class of premotor interneurons (CiDs) is largely complementary at a segmental level to that of MCoDs

The absence of MCoD activity at higher swimming frequencies raises the question of which premotor neurons drive motor output at higher frequencies. Earlier work showed that CiD interneurons, premotor excitatory neurons with descending ipsilateral axons, are engaged during fast escapes and at higher swimming frequencies 23, 24. We directly explored the relative patterns of activity in the two cell types by recording from pairs of MCoDs and more dorsal CiDs in the same body segment to compare their activity within individual bouts of evoked swimming (n = 4 pairs), as shown in Figure 7a. The activity of the two cells in a pair was largely non-overlapping. The CiD was active at the highest frequencies in the beginning of a bout and the MCoD became active at slower frequencies after the CiD firing had largely ceased (Fig. 7b). Quantification revealed that the swimming frequency at which the switch occurred varied from bout to bout, however, within swimming bouts, MCoDs and dorsal CiDs in the same segment rarely fired cyclically over the same frequency range (Fig. 7c). When they did fire occasionally during one burst at transitions from rhythmic firing in one to the other, the MCoD fired in advance of the CiD (about 0.18 ±0.1 of a cycle n=12), but not in opposite phase (Fig. 7b). These observations indicate that, within a segment, the activity of MCoDs and dorsal CiDs is largely complementary, with MCoDs silent at higher frequencies when the CiDs are engaged, and vice versa. This clear relationship would be blurred if different bouts were pooled, because of the variability in the exact frequency of the switch from trial to trial (Fig. 7c).

Shifts in the active population within a class of interneurons (CiDs) as swimming frequency increases

The inhibition of MCoDs at higher swimming speeds, as the more dorsal CiD neurons are recruited, might simply represent an inhibitory switch of cell types used for slow versus fast swimming, rather than a broad pattern of inhibition of excitatory premotor interneurons involved in slower speeds when those driving faster ones are active. We examined this by exploring the pattern of activity within a class of interneurons, the CiDs, located at different dorso-ventral positions in cord. Our previous work showed that unlike the ventral MCoDs, the CiDs are spread over a broader dorso-ventral range of the spinal cord and show a recruitment pattern from ventral to dorsal within the population as the frequency of swimming increases 23. In that work there was no relationship between soma size and recruitment. Here, we used a transgenic line with the transcription factor *alx* driving GFP expression 25, which labels CiD interneurons, to extend the sampling of the CiD population from our earlier work to include the most ventral CiDs as well as the dorsal-most excitatory CiD interneurons, which are displaced dorsally from the bulk of the CiD population. Both of these extremes in the distribution of the population were not well represented in our previous work because they are more interspersed with other cell types and thus harder to target blindly. The cells at the extremities follow the same recruitment pattern as the rest of the CiDs, with the ventral ones recruited at the lowest frequencies at which CiDs are engaged and the displaced dorsal ones active during very strong movements in larvae, as shown previously in embryos 25. There was no systematic relationship between soma size and recruitment in the entire CiD population. Removal of the displaced dorsal CiDs,

however, led to a size/recruitment relationship in the remaining CiDs that was not evident in our earlier work, probably because the transgenic line allowed us to sample more ventral, smaller neurons in the population. This relationship is not evident in the pool as a whole because the displaced dorsal neurons are also relatively small (compare Fig. 8a, f, k).

If the CiD population as a whole showed an inhibitory pattern like that between the CiD and MCoD populations, we might expect that as more dorsal CiDs are recruited, activity in the ventral ones, involved in slower movements, would decline. Indeed, we observed that some of the CiDs were silent at faster swimming speeds, but active during slow ones. If current was injected into these CiDs to depolarize them during a swimming episode, we found that the lack of activity at high frequencies was associated with a hyperpolarization of the neuron (Supplementary Fig. 2), The hyperpolarization declined at lower frequencies of swimming when the cell fired. This is consistent with some CiDs being actively inhibited at higher frequencies, like the MCoDs.

To explore the overall pattern of inhibitory interactions both within the CiD population as well as relative to the MCoDs, we divided the excitatory interneurons into four groups: 1) MCoDs, 2) CiDs that were silenced at higher swimming speeds, 3) CiDs in the main population in which silencing was not as evident upon visual inspection, and 4) the most dorsal CiDs, that were displaced from the main population. We found that during evoked swimming, the most dorsal groups of CiDs are those active initially at the highest frequencies, when more ventral CiDs and the MCoDs are not firing (Fig. 8a, b, f, g). As the frequency slows, the dorsal neurons go silent and the more ventral CiDs begin to fire (Fig. 8k, l). The probability of these ventral CiDs firing drops at the lowest frequencies, when the MCoDs are engaged (Fig. 8p, q).

This overall pattern is shown for 10 or more neurons in each group in Figure 8, which shows the dorsoventral position of the neurons (Fig. 8c, h, m, r), how their spike number changes with frequency (Fig. 8d, i, n, s), and the percentage of the time that the different classes of neurons are active over different frequency ranges (Fig. 8e, j, o, t). The MCoDs and some of the most ventral CiDs are active over the lowest frequency ranges, but their spiking drops to zero at the highest frequencies (Fig. 8n, s). Like MCoDs, ventral CiDs receive sub-threshold, phasic excitation that is masked by inhibition at high speeds (Fig. 8l). The dorsal CiDs are not active at lower frequencies, but increase their firing as the swimming frequency rises (Fig. 8i), and the displaced CiDs fire most reliably at the highest swimming frequencies (Fig. 8d). Importantly, histograms of the percentage of the cycles at each frequency in which a neuron fired at least once show that the MCoD neurons are most active at the lowest frequencies (Fig. 8t), followed by the most ventral portion of the CiD population (Fig. 8o), then CiDs just dorsal to them (Fig. 8e) and finally the displaced CiDs as the frequency of swimming increases (Fig. 8j). Within CiDs and across the MCoD/CiD populations, the probability of firing of ventral cells active at low swimming frequencies dropped at higher frequencies as new sets of neurons were recruited. Although most of our data were obtained from bouts of swimming in which frequency was slowing down (because these were more readily produced), in recordings during increases in swimming frequency, CiD and MCoD neurons active at low frequencies were silenced as the frequency of swimming rose (not shown). We conclude that the set of active premotor excitatory neurons continuously shifts

with changes in the frequency of swimming as previously active neurons are silenced when new ones are recruited.

Discussion

Our understanding of recruitment within pools of spinal neurons is largely limited to motoneurons. These neurons follow a very orderly pattern, the size principle, in which increases in the speed or forcefulness of movement are accompanied by the recruitment of additional, larger motoneurons with larger and faster motor units 4. As more motoneurons are recruited, those involved in weaker movements remain active to also contribute to the faster and stronger movements. As a result, the active pool of motoneurons continues to increase with force output as increasingly more neurons are added to the recruited pool. We show that pattern is also evident in the spinal motoneurons of zebrafish in which neurons are recruited largely by size and those active at low frequencies of swimming continue to be active at higher ones along with newly recruited motoneurons.

Our previous work showed that interneuronal recruitment order is not related to soma size, as it is among motoneurons 23, and this is confirmed here in a more extensive data set from the entire CiD population which could be targeted more specifically in a transgenic line. Although there is some size-related recruitment in the more ventral group of the CiD cells (the lower frequency ones, which we can sample more easily than before in the transgenic line), if the whole set of cells is included, the size relationships break down. Therefore, unlike the pattern of recruitment of motoneurons across species, the interneurons do not show a strict size related recruitment.

In a previous study focused on the most dorsal CiD interneurons that were activated in rapid escape bends, we found very little recruitment in this subset of the neurons for weak and strong forms of the escape 24. Instead, most neurons fired in both, with fewer spikes in weaker escapes than strong ones. That study examined only the fastest of movements (escape bends), rather than the whole range of possible bending speeds. The conclusion that nearly all of the most dorsal cells are active during fastest movements is consistent with what we found here. In the upper extreme of the recruitment range in swimming, as well as during escapes, changes in movement are probably determined by spike number, rather than changes in the extent of the active pool.

The major conclusion of the present work is that the pattern of recruitment among excitatory premotor interneurons underlying swimming in zebrafish differs in a fundamental respect from the classic pattern in motoneurons. Our earlier work showed that as swimming frequency increased, excitatory interneurons in the spinal cord, like motoneurons, were recruited in a topographic manner from ventral to dorsal 23. There were indications, however, that there might be a major difference in the recruitment pattern because unlike motoneurons, some interneurons active at low frequencies appeared to be silent at higher ones. Here we show through an analysis of the behavior, synaptic drive, and activity patterns, that as more dorsal interneurons are engaged, the more ventral ones are silenced, resulting in a shift in the distribution of the populations of active cells with speed. As the swimming frequency changes from the slowest, spontaneous swimming movements to

intermediate swimming frequencies, the active premotor neurons shift cell types from a commissural descending excitatory type (MCoD) to an ipsilateral descending excitatory class (CiD). At even higher swimming frequencies, the active cells within the CiD population change as more dorsal CiD interneurons are engaged and ventral ones are silenced. Thus, the shift of active neurons occurs both between the different classes of premotor excitatory interneurons and within a class that contains neurons active over a broad range of swimming frequencies.

Importantly, in spite of the constant shifting of the active set of interneurons with increases or decreases in the frequency of swimming movements, the movements themselves remain smooth, without evidence of any discontinuities. This may be a consequence of a gradual movement of the wave of recruitment through the population of neurons along the dorsoventral axis of the spinal cord as the frequency changes during swimming. This wave might produce a continuous, smooth handoff of the active set of neurons, rather than an abrupt transition from one set of cells to another.

What might explain the difference in the patterns of recruitment of motoneurons and excitatory interneurons? At high frequencies of swimming, both ventral motoneurons innervating slow muscle fibers and dorsal ones innervating fast fibers are activated together. In contrast, among interneurons, those active at slower frequencies are silenced during fast swimming. One possible explanation for this difference is that at the level of the muscle, a synchronous activation of the slowest and fastest muscle fibers may be important during fast movements. For instance, the slow fibers, although relaxing slowly in a way that might be expected to interfere with fast movements, contribute to a stiffening of the muscle that might match its properties to the fast oscillations required during rapid movements. The larger motoneurons and bigger groups of muscle fibers they innervate produce strong enough forces to overcome the resistance posed by the weaker slow contracting fibers, allowing movements to be superimposed on top of the stiffening produced by slower fibers.

The situation with spinal interneurons is very different. We know from ablation studies that MCoDs and dorsal CiD neurons are critical for producing proper swimming at the different speeds at which they are engaged, because ablation of the neurons involved at the slowest frequencies impairs slow swimming without affecting faster movements and vice versa 23, 30. The pattern of recruitment implies that activity in those premotor interneurons active at lower frequencies might conflict with network function at higher frequencies, necessitating their removal from the active network. Obvious sources of potential conflict include differences in the firing properties, the extent of axonal output, the connectivity, and the synaptic properties of neurons active at different frequencies of swimming. Such differences might preclude the effective use of only one set of neurons to drive the motoneurons over the entire range of swimming frequencies. For example, involvement of the entire pool at faster speeds might lead to inappropriate timing of synaptic inputs along the body due to differences in the properties of the interneurons in the population. Inappropriately timed inputs from different neurons might shunt other inputs with major consequences for the patterning of output 31. In addition, as swimming frequency rises, the speed of propagation of the wave of activity along the body increases, so neuronal features might be matched to a

narrow range of either burst rates or speed of propagation of the bending, and be incompatible with others. This might require changes in the active populations.

Whatever the explanation for the different patterns in interneurons versus motoneurons, our data show that the principles of recruitment among interneurons can differ from those for motoneurons. The results have implications not only for the general organization of motor networks, but also for our understanding of central pattern generators. The conventional wisdom regarding central pattern generators for swimming does not incorporate switches in the set of active neurons driving different speeds of locomotion. This is probably because the model systems used to reveal components of the swimming CPGs examined swimming during stable periods of motor output 9, 10. As a result, while they led to very important discoveries of neurons that likely underlie pattern generation over a relatively narrow range of speeds, they would not have detected the switches we have observed during dynamic changes in speed. We should emphasize that the shifts we found are more sophisticated than a simple switch between two very different circuits driving two different motor patterns 21. The switch from MCoDs to CiDs, might suggest such a simple network change. The shifts occur, however, even within the CiDs population, a type defined based upon transcription factor, morphology, transmitter phenotype and connectivity with motoneurons. This indicates that there may be more of a continuum of properties and wiring within the pattern generating networks that allows for a smooth change both across and within cell types in networks, and a concomitant smooth gradation of the motor pattern, swimming frequency and swimming speed. A continuous change of the CPG elements with gradations of movement frequency would stand in contrast to the notion of a discrete CPG for swimming that drives a whole range of swimming speeds.

At present, most of the data we have for spinal interneuronal recruitment patterns comes from larval zebrafish, so whether the pattern we found applies to adult fish or even more broadly among vertebrates is unknown. We do know that in adult goldfish and zebrafish, motoneurons and interneurons perform the same functions as morphologically similar neurons in zebrafish larvae, although the frequency range of swimming is slower 32-35. This, combined with the universality of the size principle of recruitment of motoneurons in vertebrates as diverse as fishes (including larval zebrafish) and humans, leads us to suspect that the pattern of recruitment of interneurons also will not be unique to larval zebrafish. The answer to the question of whether it will represent as important and broad a pattern as the size principle rests upon studies of other species, where the same question is more difficult to address.

Methods

Fish care

All experiments were performed on 4-5 day old zebrafish (*Danio rerio*) obtained from a laboratory stock of wild type adults. Embryos were raised at 28.5 °C in the same system as adults (Aquatic Ecosystems, Inc., Apopka, FL) until they became freely swimming (4 days) and then experiments were performed at room temperature (~22-26 °C). At these ages, larval fish are still nourished by the remnants of their yolk sac. All procedures conform to

the National Institutes of Health guidelines regarding animal experimentation and were approved by Cornell University's Institutional Animal Care and Use committee.

High-speed kinematics

Larvae were filmed within a Petri dish (60 × 15 mm, Falcon, VWR International, West Chester, PA) containing Hank's solution (ionic composition in mmol l^{-1}: 137 NaCl, 5.4 KCl, 0.25 Na_2HPO_4, 0.44 KH_2PO_4, 1.3 $CaCl_2$, 1.0 $MgSO_4$, 4.2 $NaHCO_3$), using a high-speed imaging system (Redlake Inc., Tucson, AZ). Bouts of swimming produced spontaneously by the fish or elicited by a tactile stimulus near the tail were filmed at a rate of 1,000 frames per second. Tail directed stimuli reliably evoked bouts of swimming that progressed in a straight direction. We omitted swimming bouts with any turning maneuvers, since this would skew our analysis of yaw. In order to capture the entire swimming bout, the field of view was expanded by fitting the camera with a lens and mounting it on a tripod well above a dissecting microscope platform. Analysis of the degree of yaw was performed automatically using custom written software (see below). Three regions along the body were selected near the head (5-15% body length), midbody (45-55% body length) and tail (85-95% body length), as determined from the midline tracking analysis (see below), and the yaw was measured for each for the duration of the bout. Selections were based on thresholded images that maximized the detection of the whole larva and were consistent between trials. For analysis, 5 evoked swimming bouts and 5 spontaneous bouts were measured from 12 different larvae.

Automated midline tracking analysis

To monitor movements, the complete midline of the fish was extracted from each film frame in which the entire image of the fish was visible. Each grayscale image was first segmented (identification of fish/non-fish pixels) using a thresholding algorithm. All pixels of lower than a threshold value are identified as the fish because the fish is darker than the background. Any background debris or experimental apparatus present in the frames was removed automatically by the software based upon size and location. The medial axis of the fish image was then extracted using the algorithm of Lee, Kashyap and Chu36. Intuitively, the medial axis captures a geometrically faithful skeleton of the zebrafish. In digitized form, it is highly sensitive to surface features and image noise. As a result, branching in the medial axis may occur. In order to elucidate the fish midline from head to tail, a modification of the medial axis was required by taking into account the geometry of the fish. Algorithms were developed to automatically eliminate branches and extrapolate the medial axis to complete tracing through the head region; details can be found in the thesis of I.Y.Y. Koh37. A Labview program fit a straight line to points extracted from different locations along the medial axis midline. Changes in the angular orientation of fitted lines at different locations (head, mid-body, tail) along the body in successive frames were used as a measure of the extent of bending in that region.

Single-cell dye electroporations and in vivo imaging

Electroporation procedures were similar to those described previously 38. Larval zebrafish were first anaesthetized in 0.02% tricaine methanesulfonate (MS-222, Sigma-Aldrich, St. Louis, MO) in Hank's solution and then embedded in a glass-bottomed dish (WillCo-dish,

WillCo Wells BV, Amsterdam, Holland) left side up in 0.4% low melting point agarose (Sigma-Aldrich) also made up in Hank's solution. The agarose was then covered in Hank's solution and the entire dish was moved to a stage equipped with an upright microscope (BX51WI, Olympus, Melville, NY). A patch micropipette (~2-4 μm diameter tip opening; see below) filled with either tetramethylrhodamine or fluorescein (3,000 molecular weight, Invitrogen-Molecular Probes, Carlsbad, CA) diluted in patch solution (10%, see below) was then carefully advanced through skin and muscle into the spinal cord using a motorized micromanipulator (Model MP-225, Sutter Instrument Co., Novato, CA) until the tip was in direct contact with the soma of the MCoD. MCoDs occupy a very distinctive, lateral position in the neuropil and so they were relatively easy to target using differential interference contrast (DIC) optics and a 40× objective lens. A brief electrical stimulus was then applied (1-5 V, 1 second train of 1 millisecond duration pulses at 100 Hz) via a silver wire within the pipette attached to an isolated pulse stimulator (Model 2100, A-M Systems Inc., Carlsborg, WA). Successful filling of the cell was quickly confirmed by switching to an epifluorescent light source. The larva was then carefully removed from the agarose and allowed to recover in Hank's solution containing 1% of the antibiotic penicillin streptomycin (Sigma-Aldrich) for at least 4-6 hours. After this time, larvae were anaesthetized again in MS-222 and re-embedded in low melting point agarose, covered in Hank's solution containing anaesthetic. Labeled cells were imaged using a confocal microscope (Zeiss LSM 510, Carl Zeiss, Inc., Thornwood, NY) and digitally reconstructed in three dimensions for analysis of axon length using NeuroLucida software (MBF Bioscience, Williston, VT).

Electrophysiological recordings

Whole-cell patch and peripheral motor nerve recordings were performed as described previously 39, 40, with minor modifications. Larvae were first anaesthetized in MS-222 and then immobilized in α-bungarotoxin (Sigma-Aldrich) dissolved in extracellular solution (0.1%, see below). After successful immobilization (5-10 minutes), larvae were transferred to a Sylgard-coated, glass bottom dish containing extracellular solution (ionic composition in mmol l^{-1}: 134 NaCl, 2.9 KCl, 1.2 $MgCl_2$, 10 HEPES, 10 glucose, 2.1 $CaCl_2$; adjusted to pH 7.8 with NaOH) and secured to the bottom using custom etched tungsten pins placed through the notocord. For recordings of the motoneuron activity from peripheral nerves, the skin was removed from the ear to just past the anus to expose the intermyotomal clefts. To record from spinal cells and motor nerves, muscle overlying one segment was additionally removed to expose the spinal cord. For paired recordings between ipsilateral MCoDs and contralateral motoneurons, the caudal-most portion of the tail was flipped over to provide access to motoneurons on the opposite side of the body. As with single neuron/motor nerve recordings, muscles overlying one segment rostrally (to target a MCoD) and one segment caudally (to target a motoneuron) were then carefully dissected away to provide access to the spinal cord. After the dissection, the dish containing the preparation was transferred to the physiological recording apparatus, where extracellular solution was constantly perfused at room temperature.

Micropipettes were created from thin walled, filamented glass capillaries (A-M Systems, Inc.) pulled on a Flaming/Brown puller (Sutter Instrument Co.). For patch recordings from

spinal cells, micropipettes were pulled to tip diameters of around 2-4 μm, yielding 10-20 MΩ resistances. For extracellular recordings of peripheral nerves, these same micropipettes were broken to make tip diameters of about 20-50 μm and polished using a microforge (Model MF-830, Narishige International USA, East Meadow, NY). Patch electrodes were first backfilled with intracellular solution (ionic composition in mmol l^{-1}: 125 K-gluconate, 2.5 $MgCl_2$, 10 EGTA, 10 HEPES, 4 Na_2ATP; adjusted to pH 7.3 with KOH) and then advanced into the exposed portion of the spinal cord using a motorized micromanipulator, while maintaining positive pressure (∼25-50 mmHg) via a pneumatic transducer (Model DPM-1B, Bio-Tek Instruments Inc., Winooski, VT) to avoid tip clogging. When the tip of the micropipette was in close proximity to the soma of the targeted cell, a GΩ seal was obtained by either equilibrating the micropipette to atmosphere or applying gentle suction. A holding current of -65 mV was then applied once the micropipette had become cell attached. At this point, we would assess the firing activity of the cells during swimming to compare with recordings obtained in whole-cell mode. Whole-cell recordings were obtained by penetrating the membrane using gentle suction pulses. Standard corrections for bridge balance and capacitance were then applied. For simultaneous motor nerve recordings, nerve micropipettes were filled with extracellular solution, lowered onto the intermyotomal clefts and gentle suction was then applied via a pneumatic transducer to obtain a tight seal. Motor nerve recordings were always from the same side of the body as the patch recording and nerve pipettes were typically placed just dorsal to the midline of the muscle segment, where the ventral root exits spinal cord, to maximize the likelihood of sampling a majority of the efferent nerve.

Whole cell and peripheral nerve recordings were acquired using a MultiClamp 700A amplifier (Molecular Devices-Axon Instruments Inc., Sunnyvale, CA), a Digidata series 1322A digitizer (Axon Instruments Inc.) and pClamp 8.2 software (Axon instruments Inc.). Electrical signals from spinal cells were filtered at 30 kHz and digitized at 63 kHz at a gain of 20 (Rf = 5 GΩ). Only cells that had stable membrane potentials at or below -40 mV were included in this study. A junction potential using this recording solution has already been calculated at 16 mV, which would result in a shift of measured potentials 16 mV in the negative direction 41. Since this would not impact on our conclusions, we did not correct for it. Extracellular signals from peripheral nerves were recorded in current clamp mode at a gain of 1,000, with the low and high frequency cutoff set at 100 and 4,000 Hz, respectively. We included a fluorescent dye in the patch solution (0.025% sulforhodamine-B acid chloride, Sigma-Aldrich) so we could assess the morphologies of the cells immediately after the recordings. Fluorescent images were acquired with a CCD camera (C-72-CCD; Dage MTI, Michigan City, IN) and a frame grabber (LG3; Scion, Frederick, MD) controlled by NIH Image software.

Swimming would often occur spontaneously, but could be more reliably elicited by flashes of light (flashlight) or a brief electrical stimulus (<1 ms in duration at 1-10 V) delivered via a tungsten electrode placed near the tail (DS2 Isolated Stimulator, Digitimer, Ltd., Welwyn Garden City, England). All data were analyzed off-line using DataView (Dr. William Heitler, University of St Andrews, St Andrews, Scotland). Measurements of swimming parameters are based on at least 5 evoked swimming bouts and 5 spontaneous swimming bouts per fish. Images of recorded cells were graphically reconstructed using Adobe

Illustrator (Adobe Systems Inc., San Jose, CA). Data are reported as means +/- standard deviation.

Supplementary Material

Refer to Web version on PubMed Central for supplementary material.

Acknowledgments

This work was supported by fellowships (NS44728 to D.L.M. and NS44758 to M.A.M.) and a grant (NS26539 to J.R.F.) from the National Institutes of Health. We are extremely grateful to Shin-ichi Higashijima for providing us with the *alx*:GFP transgenic fish. We also thank Lindsay Heller for fish care and Minoru Koyama for comments on the manuscript.

References

1. Mendell LM. The size principle: a rule describing the recruitment of motoneurons. J Neurophysiol. 2005; 93:3024–3026. [PubMed: 15914463]
2. Cope TC, Sokoloff AJ. Orderly recruitment among motoneurons supplying different muscles. J Physiol Paris. 1999; 93:81–85. [PubMed: 10084711]
3. Cope TC, Pinter MJ. The size principle: Still working after all these years. News in Physiological Sciences. 1995; 10:280–286.
4. Henneman E, Somjen G, Carpenter DO. Functional Significance of Cell Size in Spinal Motoneurons. J Neurophysiol. 1965; 28:560–580. [PubMed: 14328454]
5. Zajac FE, Faden JS. Relationship among recruitment order, axonal conduction velocity, and muscle-unit properties of type-identified motor units in cat plantaris muscle. J Neurophysiol. 1985; 53:1303–1322. [PubMed: 2987433]
6. Hill AA, Cattaert D. Recruitment in a heterogeneous population of motor neurons that innervates the depressor muscle of the crayfish walking leg muscle. The Journal of experimental biology. 2008; 211:613–629. [PubMed: 18245639]
7. Davis WJ. Functional significance of motorneuron size and soma position in swimmeret system of the lobster. J Neurophysiol. 1971; 34:274–288. [PubMed: 4251022]
8. Gabriel JP, Scharstein H, Schmidt J, Buschges A. Control of flexor motoneuron activity during single leg walking of the stick insect on an electronically controlled treadwheel. J Neurobiol. 2003; 56:237–251. [PubMed: 12884263]
9. Grillner S. Biological pattern generation: the cellular and computational logic of networks in motion. Neuron. 2006; 52:751–766. [PubMed: 17145498]
10. Roberts A, Soffe SR, Wolf ES, Yoshida M, Zhao FY. Central circuits controlling locomotion in young frog tadpoles. Ann N Y Acad Sci. 1998; 860:19–34. [PubMed: 9928299]
11. Stein PS, McCullough ML, Currie SN. Spinal motor patterns in the turtle. Ann N Y Acad Sci. 1998; 860:142–154. [PubMed: 9928308]
12. Kiehn O. Locomotor circuits in the mammalian spinal cord. Annu Rev Neurosci. 2006; 29:279–306. [PubMed: 16776587]
13. Roberts A, Kahn JA, Soffe SR, Clarke JD. Neural control of swimming in a vertebrate. Science. 1981; 213:1032–1034. [PubMed: 7196599]
14. Cohen AH, Wallen P. The neuronal correlate of locomotion in fish. “Fictive swimming” induced in an in vitro preparation of the lamprey spinal cord. Exp Brain Res. 1980; 41:11–18. [PubMed: 7461065]
15. Grillner S, McClellan A, Sigvardt K, Wallen P, Wilen M. Activation of NMDA-receptors elicits “fictive locomotion” in lamprey spinal cord in vitro. Acta Physiol Scand. 1981; 113:549–551. [PubMed: 6291323]

16. Kudo N, Yamada T. N-methyl-D,L-aspartate-induced locomotor activity in a spinal cord-hindlimb muscles preparation of the newborn rat studied in vitro. Neurosci Lett. 1987; 75:43–48. [PubMed: 3554010]
17. Smith JC, Feldman JL. In vitro brainstem-spinal cord preparations for study of motor systems for mammalian respiration and locomotion. J Neurosci Methods. 1987; 21:321–333. [PubMed: 2890797]
18. Sillar KT, Roberts A. Control of frequency during swimming in Xenopus embryos: a study on interneuronal recruitment in a spinal rhythm generator. J Physiol. 1993; 472:557–572. [PubMed: 8145161]
19. Li WC, Sautois B, Roberts A, Soffe SR. Reconfiguration of a vertebrate motor network: specific neuron recruitment and context-dependent synaptic plasticity. J Neurosci. 2007; 27:12267–12276. [PubMed: 17989292]
20. Berkowitz A. Spinal interneurons that are selectively activated during fictive flexion reflex. J Neurosci. 2007; 27:4634–4641. [PubMed: 17460076]
21. Budick SA, O'Malley DM. Locomotor repertoire of the larval zebrafish: swimming, turning and prey capture. The Journal of experimental biology. 2000; 203:2565–2579. [PubMed: 10934000]
22. Thorsen DH, Cassidy JJ, Hale ME. Swimming of larval zebrafish: fin-axis coordination and implications for function and neural control. The Journal of experimental biology. 2004; 207:4175–4183. [PubMed: 15531638]
23. McLean DL, Fan J, Higashijima S, Hale ME, Fetcho JR. A topographic map of recruitment in spinal cord. Nature. 2007; 446:71–75. [PubMed: 17330042]
24. Bhatt DH, McLean DL, Hale ME, Fetcho JR. Grading movement strength by changes in firing intensity versus recruitment of spinal interneurons. Neuron. 2007; 53:91–102. [PubMed: 17196533]
25. Kimura Y, Okamura Y, Higashijima S. alx, a zebrafish homolog of Chx10, marks ipsilateral descending excitatory interneurons that participate in the regulation of spinal locomotor circuits. J Neurosci. 2006; 26:5684–5697. [PubMed: 16723525]
26. Ritter DA, Bhatt DH, Fetcho JR. In vivo imaging of zebrafish reveals differences in the spinal networks for escape and swimming movements. J Neurosci. 2001; 21:8956–8965. [PubMed: 11698606]
27. Hale ME, Ritter DA, Fetcho JR. A confocal study of spinal interneurons in living larval zebrafish. The Journal of comparative neurology. 2001; 437:1–16. [PubMed: 11477593]
28. Higashijima S, Schaefer M, Fetcho JR. Neurotransmitter properties of spinal interneurons in embryonic and larval zebrafish. The Journal of comparative neurology. 2004; 480:19–37. [PubMed: 15515025]
29. Frankenhaeuser B, Hodgkin AL. The action of calcium on the electrical properties of squid axons. J Physiol. 1957; 137:218–244. [PubMed: 13449874]
30. Fan, J.; Hale, ME. Soc. Neurosci. Abstr. Viewer/Itinerary Planner. Society for Neuroscience; Washington DC: 2005. Excitatory descending spinal interneurons influrence the degree of axial bending during startles of larval zebrafish. Program 751.14http://sfn.scholarone.com/itin2005/
31. Fetcho JR. Morphological variability, segmental relationships, and functional role of a class of commissural interneurons in the spinal cord of goldfish. The Journal of comparative neurology. 1990; 299:283–298. [PubMed: 2229481]
32. Liu DW, Westerfield M. Function of identified motoneurones and co-ordination of primary and secondary motor systems during zebra fish swimming. J Physiol. 1988; 403:73–89. [PubMed: 3253426]
33. Fetcho JR, Faber DS. Identification of motoneurons and interneurons in the spinal network for escapes initiated by the mauthner cell in goldfish. J Neurosci. 1988; 8:4192–4213. [PubMed: 3183720]
34. Svoboda KR, Fetcho JR. Interactions between the neural networks for escape and swimming in goldfish. J Neurosci. 1996; 16:843–852. [PubMed: 8551364]
35. Gabriel JP, et al. Locomotor pattern in the adult zebrafish spinal cord in vitro. J Neurophysiol. 2008; 99:37–48. [PubMed: 17977928]

36. Lee T-C, Kashyap RL, Chu C-N. Building skeleton models via 3-D medial surface/axis thinning algorithms. BVGIP: Graph. Models Image Process. 1994; 56:462–478.

37. Koh, IYY. PhD Thesis. Department of Applied Mathematics and Statistics, Stony Brook University; 2001. Automated Recognition Algorithms for Neural Studies.

38. Bhatt DH, Otto SJ, Depoister B, Fetcho JR. Cyclic AMP-induced repair of zebrafish spinal circuits. Science. 2004; 305:254–258. [PubMed: 15247482]

39. Drapeau P, Ali DW, Buss RR, Saint-Amant L. In vivo recording from identifiable neurons of the locomotor network in the developing zebrafish. J Neurosci Methods. 1999; 88:1–13. [PubMed: 10379574]

40. Masino MA, Fetcho JR. Fictive swimming motor patterns in wild type and mutant larval zebrafish. J Neurophysiol. 2005; 93:3177–3188. [PubMed: 15673549]

41. Higashijima S, Masino MA, Mandel G, Fetcho JR. Engrailed-1 expression marks a primitive class of inhibitory spinal interneuron. J Neurosci. 2004; 24:5827–5839. [PubMed: 15215305]

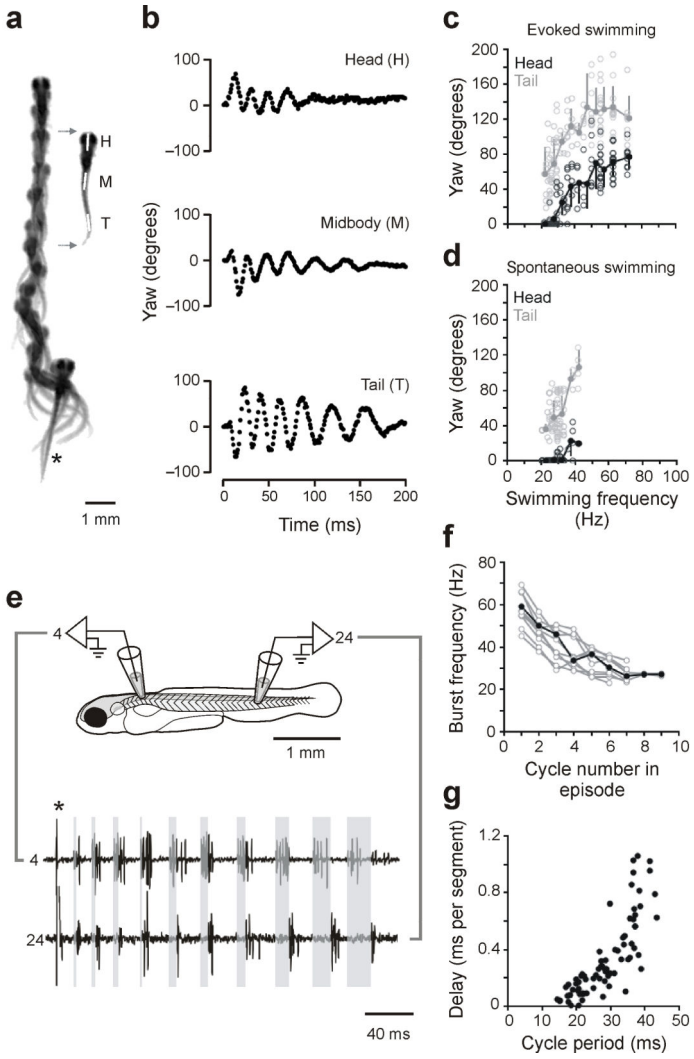

Figure 1. Analysis of real and fictive evoked swimming movements

(a) Consecutive overlapping images of a bout of swimming elicited by a tactile stimulus to the tail (at asterisk). A frame extracted from the montage (gray arrows) shows the regions selected for kinematic analysis, at the head (H), midbody (M) and tail (T). Images were captured at 1,000 Hz (images 1-9, every 4 ms; 10-12, 8 ms; 13-14, 16 ms; 15-18, 32 ms).

(b) Automated analysis of yaw at three points along the body, from the swimming bout illustrated in **a**. Only the tail is showing any noticeable movement at the end of the bout, when swimming is slowest.

(c) Plots of head and tail yaw from 12 evoked swimming bouts in 12 larvae. The degree of head and tail yaw decreases as a function of swimming frequency. Open circles are raw data points, while closed circles represent means (plus or minus standard deviations) from data binned at 5 Hz intervals (e.g., 15-20, 20-25, etc...). For simplicity, only the first episode of the five analyzed in each fish is illustrated here and in **d** (see Methods).

(d) A similar plot for spontaneous bouts of swimming (12 from the same 12 larvae), whose values are comparable to the lower end of evoked swimming frequencies.

(e) Fictive swimming activity recorded from motor nerves along the same side of the body (4^{th} and 24^{th} muscle cleft on the left side), whose location is illustrated schematically. A brief electrical stimulus (artifact at asterisk) was used to elicit swimming activity. Shaded gray boxes from the start of the burst in the rostral segment to the start of the caudal burst in the same cycle demonstrate the gradual increase in longitudinal delay associated with a smooth decrease in swimming frequency.

(f) Plot of motor nerve burst frequency (measured from the tail) with respect to the cycle in a bout, from 10 bouts in 10 larvae.

(g) Plot of longitudinal delay with respect to cycle period, from the same 10 bouts in **f**.

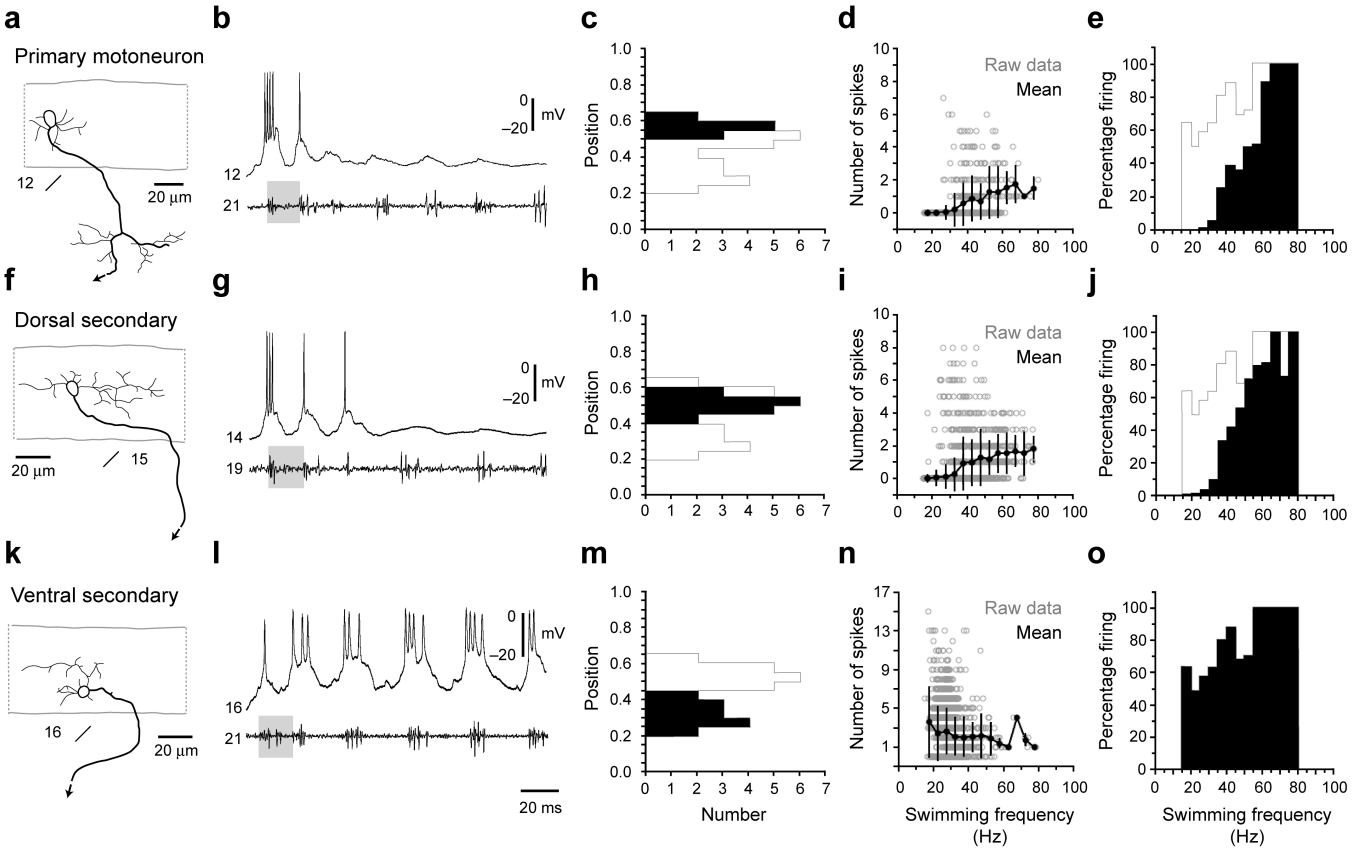

Figure 2. Recruitment pattern of spinal motoneurons

(a-e) Data from primary motoneurons are organized according to morphology (**a**), physiology (**b**), dorso-ventral soma position (**c**), number of spikes during swimming at different frequencies (**d**) and reliability of firing during swimming at different frequencies (**e**). In **a**, a black arrow indicates continuation of the axon. Segment locations are noted below the images. In **b**, gray shaded boxes are present to illustrate a similar swimming frequency. Segmental recording locations are noted to the left of the trace. For reference, in **c** and **e**, a gray outline shows the maximum values of the histogram one would get if those for the individual groups of neurons were overlain. In **d**, open circles are raw data points, while closed circles represent means (plus and minus standard deviations) from data binned at 5 Hz intervals, using the nerve recording as a frequency reference. In **e**, the number of cycles in which a cell fired is expressed as a percentage of the total number of cycles at that frequency. Plots are derived from 173 bouts from 10 cells in 10 larvae.

(f-j) Data from dorsally located secondary motoneurons (> 0.42) are organized as detailed in **a-e**. Plots are derived from 317 bouts from 16 cells in 16 larvae.

(k-o) Data from more ventrally located secondary motoneurons (< 0.42) are organized as detailed in **a-e**. Plots are derived from 187 bouts from 14 cells in 14 larvae.

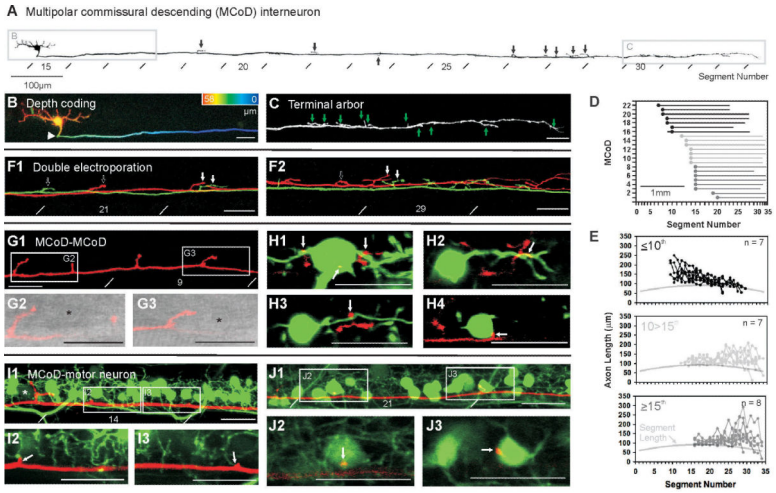

Figure 3. Anatomy of multipolar commissural descending (MCoD) interneurons

(a) Inverted fluorescent image of a dye-filled MCoD created from successive confocal images along the body. Black arrows indicate axon collaterals, lines indicate myomeric segmental boundaries.

(b) The contralateral axonal projection characteristic of MCoDs is illustrated here by pseudocoloring the region in **a** according to depth (red is distal and blue is proximal, total depth is 58 µm).

(c) Magnification of the region indicated in **a** provides a more detailed view of axon collaterals (at green arrows). This image is created from a collapsed Z-stack 18 µm in thickness.

(d) Plot of the length of descending axons for 22 electroporated MCoDs. The X-axis has been normalized according to the length of each muscle segment.

(e) Plots of axon lengths per segment (in micrometers) for MCoDs located in three defined segmental regions (as indicated on the respective plots). Here, the X-axis has not been normalized to segment lengths. For comparison, a gray line indicates the length of each segment.

(f-g) MCoDs located in either the 9^{th} (red) and 11^{th} (green) segments (**f**) or the 14^{th} (red) and 15^{th} (green) segments (**g**) were electroporated with different wavelength dyes to examine the relationship of axon collaterals. White arrows indicate potential sites of convergence, while open arrows indicate likely sites of divergence. **f** is a collapsed Z-stack 9 µm thick, while **g** is 14 µm thick.

(h-j) A confocal image of a MCoD electroporated in the 7^{th} segment (**h**), when combined with differential interference contrast (DIC) light microscopy (**i** and **j**), reveals the proximity of axon collaterals to somata located laterally in the neuropil (at asterisks), where they might contact processes arising from the somata. **h** is a collapsed Z-stack 12 µm thick, while **i** and **j** are single 1 µm optical sections.

(k-n) Confocal images of an electroporated MCoD (red) from the 9^{th} segment and back-filled MCoDs (green) from the 13^{th} **(k),** 14^{th} **(l),** 15^{th} **(m)** and 16^{th} (**n**) segments reveal the proximity of MCoD axon collaterals (at white arrows) to the dendrites and somata of more caudal MCoDs on the opposite side of the body. Images are single 1 µm optical sections.

(o-q) Confocal images of Islet-1 GFP (green) labeled secondary motoneurons and an electroporated MCoD (red) from the 12th segment. The MCoD axon runs along the ventral extent of the dendritic zone **(o),** where it appears to make contact with dendrites (**p** and **q**). **o** is a collapsed Z-stack 13 μm thick, while **p** and **q** are single 1 μm optical sections. **(r-t)** Confocal images as described in **o-q**, but nearer the tail. The MCoD here is from the 13th segment. More caudally, the MCoD axon runs at the level of secondary motoneuron somata (**r**), where axon collaterals appear to make direct somatic contact (**s** and **t**). **r** is a collapsed Z-stack 15 μm thick, while **s** and **t** are single 1 μm optical sections. All scale bars are 20 μm, unless labeled.

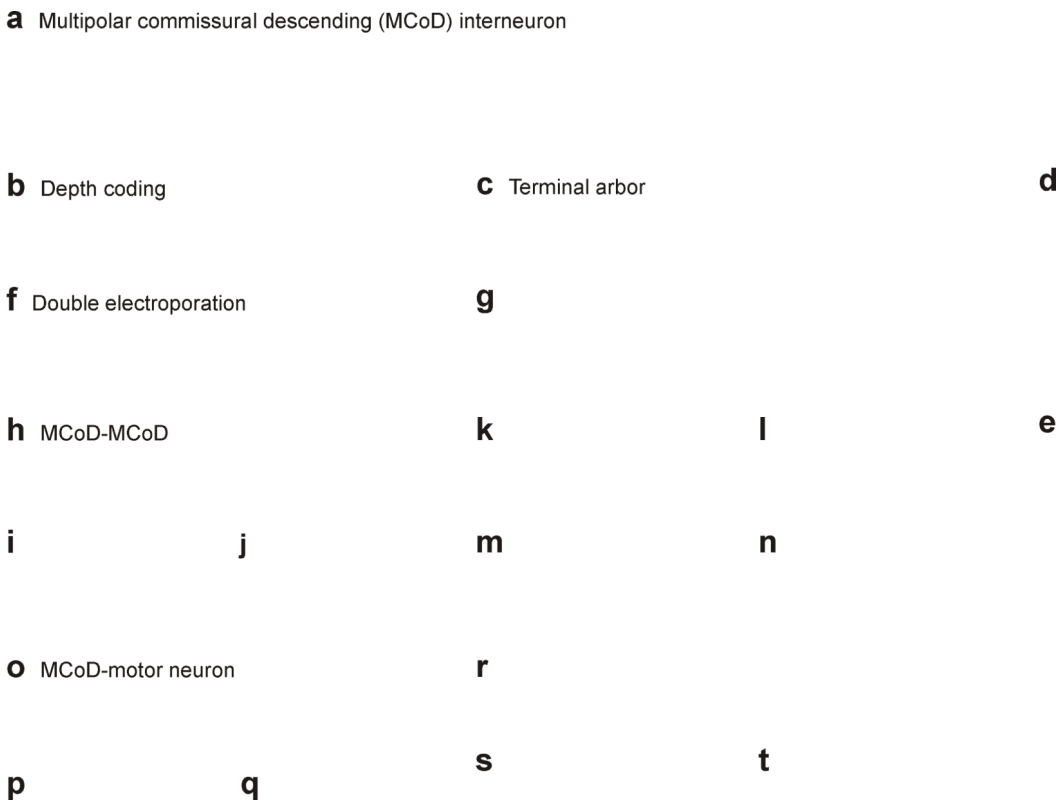

Figure 4. Pair-wise recordings of MCoDs and motoneurons

(a) Graphic reconstructions of the connected MCoD and secondary motoneuron (smn; see top schematic for respective location), whose physiology is illustrated in **b**. The MCoD axon crosses the spinal cord (at asterisk) and descends contralaterally (gray). The secondary motoneuron axon was torn during the dissection (asterisk). Segment locations are indicated below the images.

(b) Five overlapping traces of post-synaptic potentials (PSPs) in a secondary motoneuron (smn) from the 29th segment following spikes generated in a MCoD from the 13th segment in control conditions (top gray trace), in high divalent cation solution (middle gray trace) and following the blockade of glutamatergic synapses with 10 μM NBQX and 100 μM APV (bottom gray trace). A black arrow highlights the likely electrical component of the PSP. For simplicity, only one action potential trace is shown (top black trace).

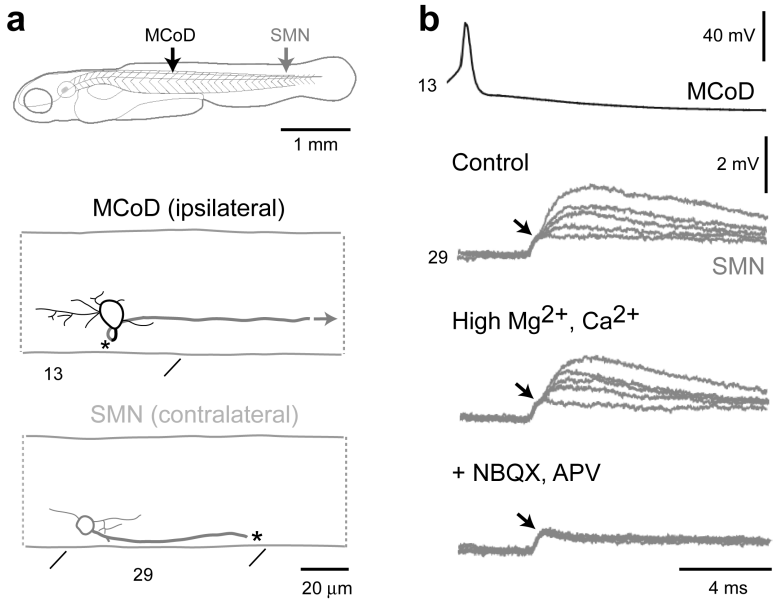

Figure 5. Rhythmic firing behavior of MCoDs during fictive swimming

(a-b) Spontaneous bouts of fictive swimming while recording from a MCoD and a motor nerve are illustrated on a slower (**a**) and faster (**b**) time base. Segmental locations are noted on the traces.

(c) Recordings of bouts of swimming from a different larva illustrate that at higher swimming frequencies MCoDs are less likely to fire action potentials.

(d) Plot of the number of spikes in a MCoD per cycle versus swimming frequency using the nerve recording as a frequency reference (287 swimming bouts in 10 larvae). Open circles are raw data points, while closed circles represent means (plus standard deviations) from data binned at 5 Hz intervals.

(e) Histogram of swimming frequency measured from nerve recordings of 1,896 cycles from 287 swimming bouts in 10 larvae.

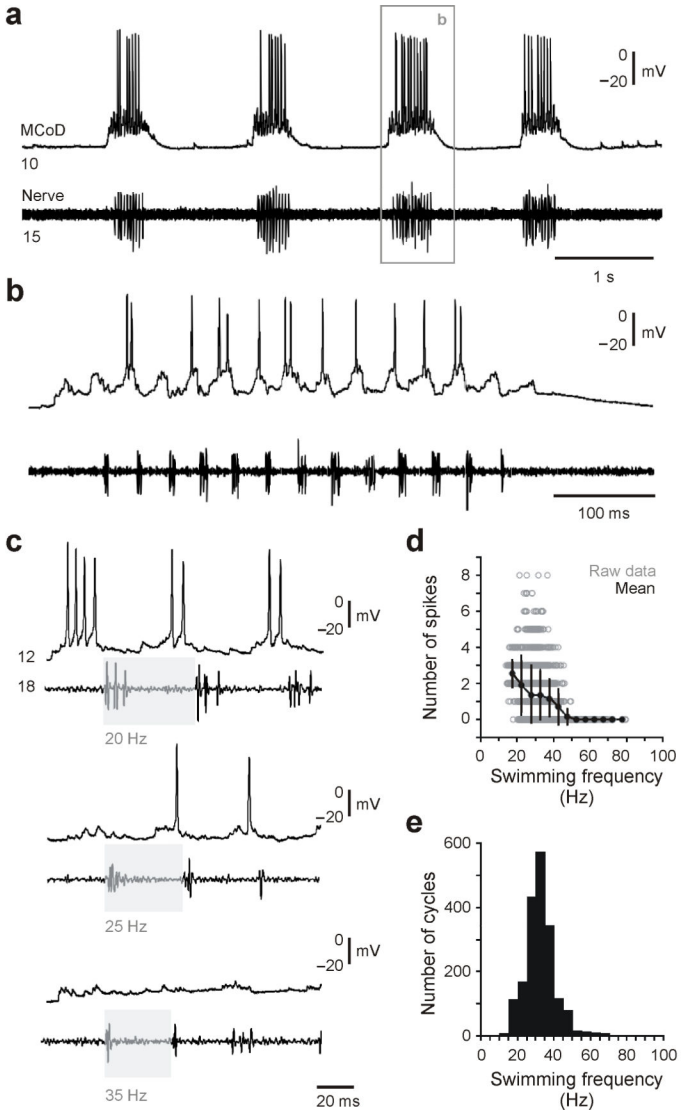

Figure 6. Inhibition of MCoDs at fast swimming frequencies

(a-b) Recordings of a MCoD and a motor nerve in response to a brief electrical stimulus (at asterisk) at two depolarized holding potentials, one using 10 pA of current (**a**) and one using 20 pA (**b**). Holding the MCoD at a more depolarized level reveals the hyperpolarizing nature of the inhibition early in the bout when the frequency of swimming is highest (at gray arrows).

(c-d) Recordings in cell-attached mode (**c**) and whole-cell mode (**d**). The MCoD is inhibited at the beginning of the episode when swimming is fastest using both approaches. Spikes in cell-attached mode are marked by black arrows. These recordings were routinely performed to make sure the inhibition was not simply an artifact of our patch recording process.

(e-h) The inhibition of the MCoD at faster swimming frequencies (**e**) can be reversibly blocked by strychnine (**f**), suggesting it is glycinergic. With prolonged exposure (**g**), strychnine also disrupts the motor pattern as assessed by the motor nerve recording. This effect is reversed when returned to control saline (**h**).

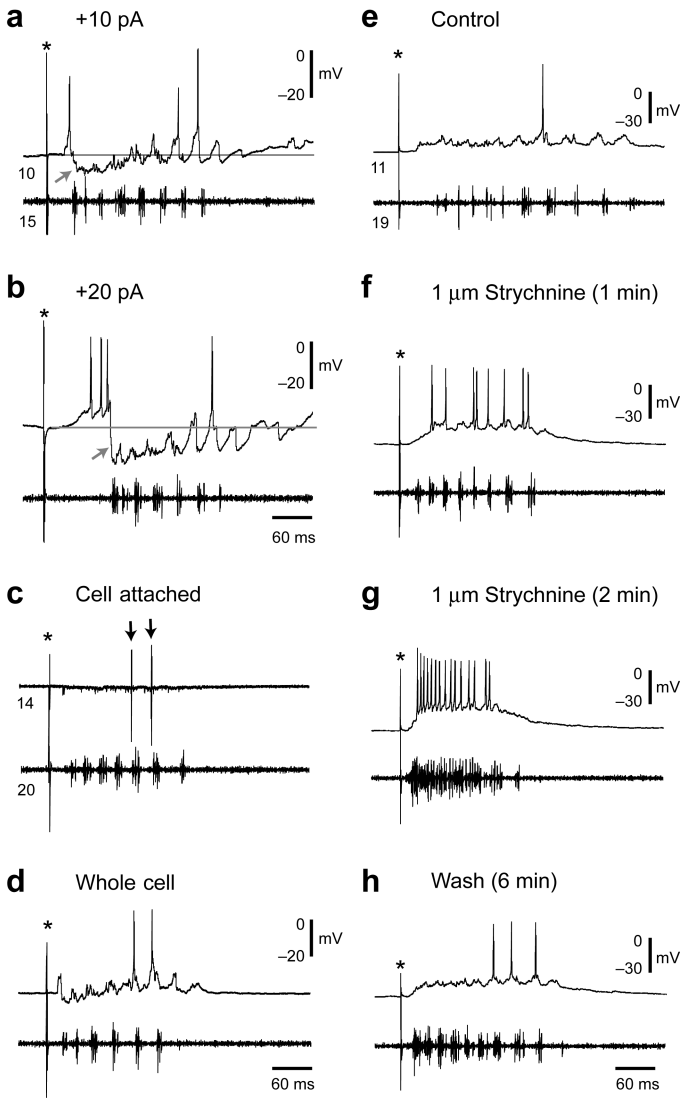

Figure 7. Dual MCoD and CiD interneuron recordings

(a) Graphic reconstructions of the MCoD (gray) and CiD (black) whose physiology is illustrated in **b**. A black asterisk indicates where the MCoD axon crosses cord, while arrows indicate the continuation of the axons.

(b) Whole-cell recordings from a MCoD and CiD in the same segment with mutually exclusive firing behavior. Simultaneous cyclical firing behavior was extremely rare (5 out of 223 cycles from 43 swimming bouts in 4 larvae). For frequency measures, cells must fire in consecutive motor bursts to be quantified. Using this criterion, events were only counted as simultaneous if the MCoD and CiD both fired cyclically, in the same two consecutive bursts of motor output. Here, gray lines mark the transition at which the CiD stopped firing and the MCoD began. In this case, the MCoD and CiD only fired together during one burst at the transition and so by our definition are not synchronous.

(c) Plot of firing of MCoD/CiD pairs in different trials versus swimming frequency, using the inter-cycle interval of the MCoD (open gray circles) or the CiD (filled black circles) firing as the frequency measure, from 43 swimming bouts in 4 larvae in which MCoD and

CiD pairs were recorded. Black boxes illustrate examples where the MCoD and the CiD fired in the same cycle, which was very rare.

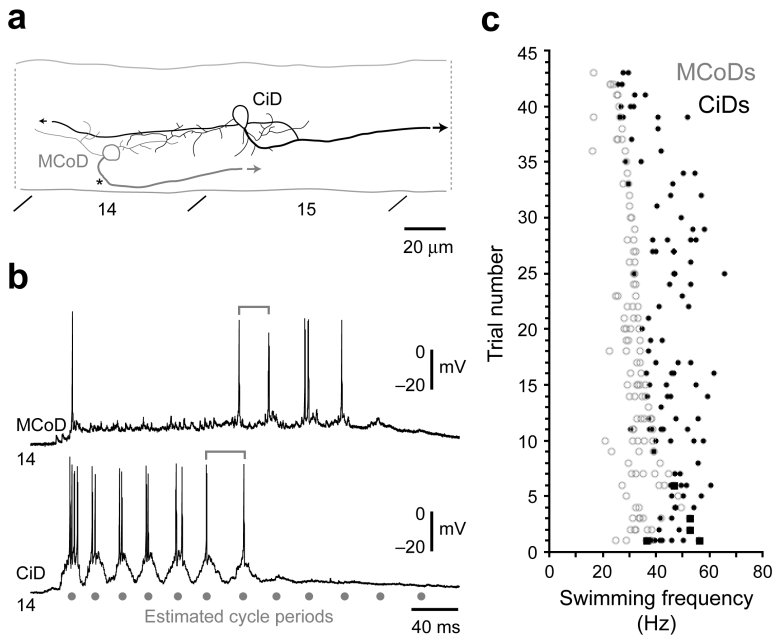

Figure 8. Frequency-dependent shifts in recruitment within and between classes

(a-e) Data from displaced, dorsally located CiD cells, the most dorsal of the CiDs, are organized according to morphology (**a**), physiology (**b**), dorso-ventral soma position (**c**), number of spikes during swimming at different frequencies (**d**) and reliability of firing during swimming at different frequencies (**e**). In **a**, black arrows indicate continuation of the axon. Segment locations are noted below the images. In **b**, gray shaded boxes are present to illustrate a similar swimming frequency. Segmental recording locations are noted to the left of the trace. For reference, in **c** and **e**, a gray outline shows the maximum values of the histogram one would get if those for the individual groups of neurons were overlain. In **d**, open circles are raw data points, while closed circles represent means (plus and minus standard deviations) from data binned at 5 Hz intervals, using the nerve recording as a frequency reference. In **e**, the number of cycles in which a cell fired is expressed as a percentage of the total number of cycles at that frequency. Plots are derived from 127 bouts from 12 cells in 12 larvae.

(f-j) Data from dorsally located, non-displaced CiD cells are organized as detailed in **a-e** Plots are derived from 268 bouts from 14 cells in 14 larvae.

(k-o) Data from more ventrally located CiD cells are organized as detailed in **a-e**. Plots are derived from 398 bouts from 11 cells in 11 larvae.

(p-t) Data from MCoD cells are organized as detailed in a-e In **p**, an asterisk marks where the axon crosses cord and then descends. The plot in **s** was first illustrated in Figure 5**d**. As the frequency of swimming increases, the active set of cells shifts from the ventral MCoDs and CiDs to the dorsal CiDs, as seen most easily by a comparison of the positions (black bars superimposed upon the whole population outlined in gray in **c, h, m, r**) with the frequencies over which they are active (black in **e, j, o, t**).

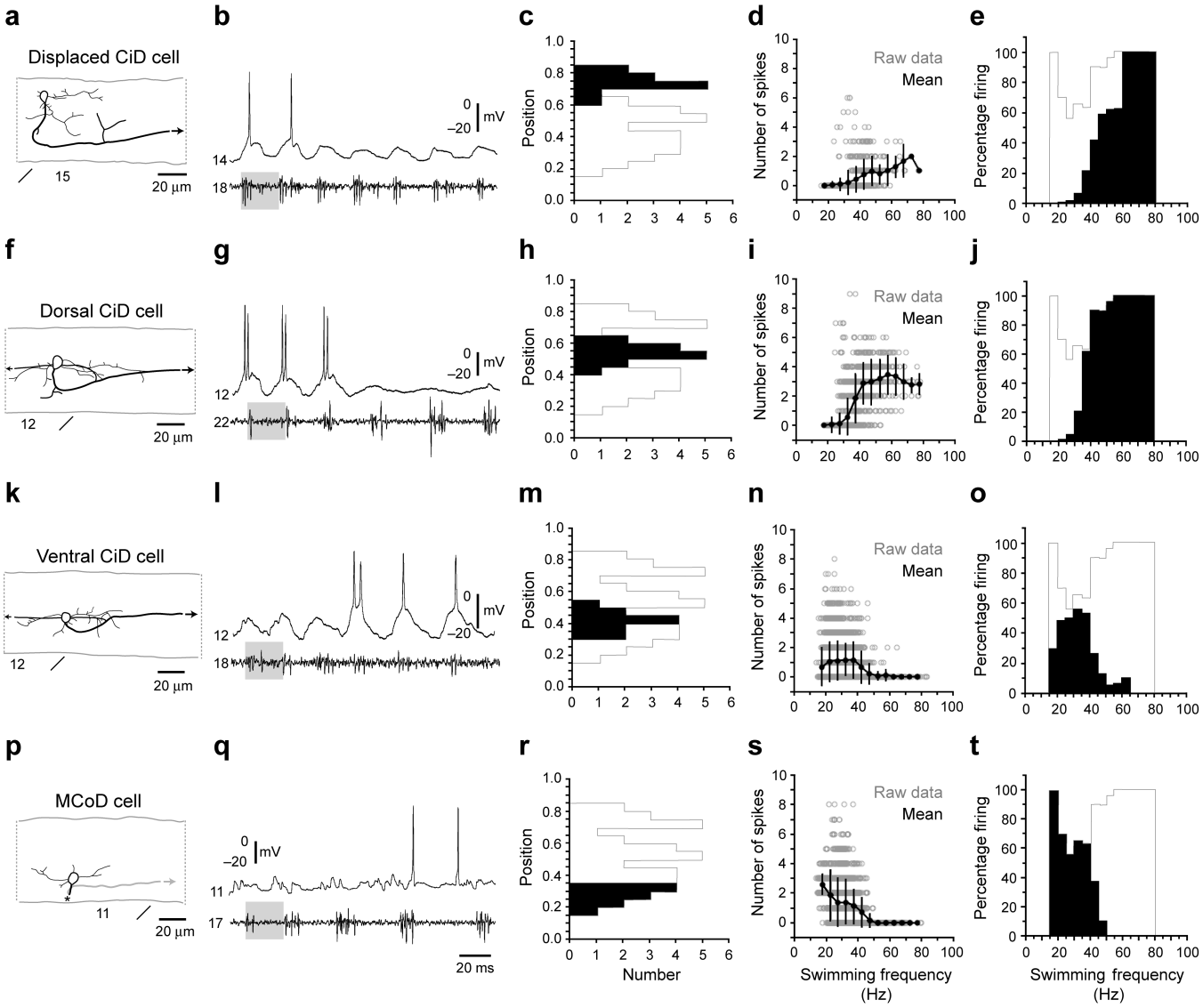

Figure 9.